This article has been accepted for inclusion in a future issue of this journal. Content is final as presented, with the exception of pagination.

18–45-GHz Sideband-Separating Downconverter With RF Image Rejection Calibration

Sitwala Mundia and Tinus Stander, *Senior Member, IEEE*

***Abstract*— We present a sideband separating downconverter for radio astronomy applications, featuring radio frequency image rejection calibration for frequencies between 18 and 45 GHz. The multichip module optimizes image rejection for specific target observation frequencies by injecting a modulated portion of the *Q*-branch signal into the *I*-branch with independent upper and lower sideband injection control. Measurements demonstrate an average image rejection ratio improvement of 9 dB over a 7-GHz band of interest compared with a baseline uncalibrated operation, with improvement of over 40 dB in targeted subbands.**

***Index Terms*— Image rejection, millimeter-wave technology, multichip modules (MCM), radio astronomy, receivers, sideband separation.**

I. Introduction

MODERN radio astronomy receivers often use sideband separating (2SB) receivers that double the observation band of a single sideband architecture [1], [2], as well as provide concurrent dual-band observation of, e.g., water and methanol maser lines [3]. In the 2SB architecture, the lower sideband (LSB) and upper sideband (USB) are obtained at two separate output channels, with the downconverter using phase cancellation to remove the unwanted sideband. However, 2SB receivers can suffer from poor sideband rejection due to imbalance in the amplitude and phase of the in-phase and quadrature (IQ) paths in the receivers attributable to component and assembly tolerances, as well as nonidentical components in the *I* and *Q* branch. The resulting finite sideband rejection can be quantified as the image rejection ratio (IRR), the ratio of the desired signal power to the image power.

A common approach to addressing this imbalance is implementing the radio frequency (RF) hybrid in the digital domain [2], [4], [5], [6], digitizing the *I* and *Q* paths separately and implementing the hybrid combiner digitally with IQ imbalance compensation [7]. This, however, limits the IF bandwidth to that of the available digitizers and increases the burden on the digital signal processing system. While improving the balance of the quadrature generation stage will also improve IRR [8], this is only an option if quadrature local oscillator (LO) control is available, and not if an off-the-shelf IQ mixer is used. Combining controlled quadrature generation with variable gain in the receiver paths can be used to calibrate a weaver architecture image reject receiver, but the method has only been demonstrated up to the L-band with baseband downconversion [9].

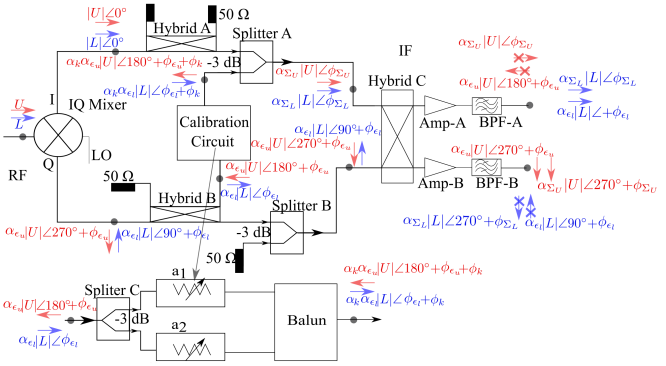

Fig. 1. Schematic of 2SB downconversion module with RF image rejection calibration. *U* (USB) and *L* (LSB) are vectors showing how signals are canceled and maximized at both the outputs.

In this letter, the sideband rejection calibration is implemented in the *I* and *Q* paths of a 2SB downconverter before digitization and the quadrature hybrid. As the calibration is performed in the analog path, it allows for IRR improvement before digitization of the signal at a high IF frequency enabling wideband correction, or narrowband correction over a designated subband, without increasing the burden on the analog-to-digital converter (ADC) or digital back-end. It also allows for IRR improvement independent of the digital back-end. The proposed downconverter is implemented as a multichip module (MCM) on RF laminate. This is an extension of previous work [10], where preliminary simulation results of the downconverter circuit were presented.

II. Proposed Downconverter Design

A. Theory of Operation

The schematic of the downconverter design, with idealized vector responses, is shown in Fig. 1. The *U* (red) and *L* (blue) vectors in Fig. 1, represent USB and LSB, respectively, with their relative phase shift in the downconverter. Ideally, at the IQ mixer, *L* and *U* will be 180° out of phase in the *Q*-branch, and recombining them at the output quadrature hybrid leads to separation of the *L* and *U* signals. However, amplitude errors α_{ϵ_u} and α_{ϵ_l} (for the USB and LSBs) and phase errors ϕ_{ϵ_u} and ϕ_{ϵ_l} exist in the downconverter due to nonideal component responses, which requires consideration of a complex error coefficient included to the *L* and *U* vectors in the *Q*-path. The

Received 28 August 2024; revised 10 November 2024; accepted 5 December 2024. This work was supported by the South African Radio Astronomy Observatory (SARAO) under Grant UID97929. *(Corresponding author: Sitwala Mundia.)*

The authors are with the Carl and Emily Fuchs Institute for Microelectronics, Department EEC Engineering, University of Pretoria, Pretoria 0028, South Africa (e-mail: sitwala.mundia@tuks.co.za).

Color versions of one or more figures in this letter are available at https://doi.org/10.1109/LMWT.2024.3514321.

Digital Object Identifier 10.1109/LMWT.2024.3514321

2771-957X © 2024 IEEE. All rights reserved, including rights for text and data mining, and training of artificial intelligence and similar technologies. Personal use is permitted, but republication/redistribution requires IEEE permission.
See https://www.ieee.org/publications/rights/index.html for more information.
Authorized licensed use limited to: University of Pretoria. Downloaded on January 15,2025 at 13:08:33 UTC from IEEE Xplore. Restrictions apply.

This article has been accepted for inclusion in a future issue of this journal. Content is final as presented, with the exception of pagination.

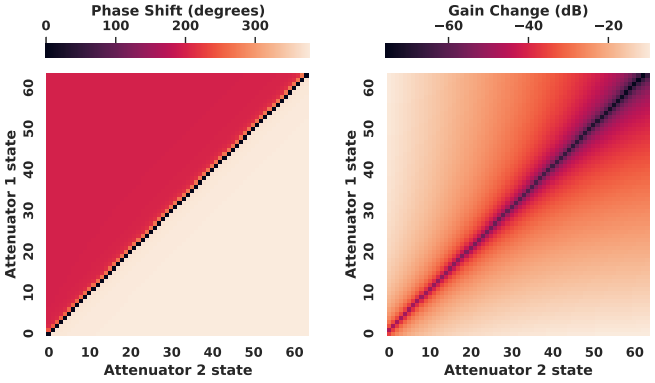

(a) (b)

Fig. 2. Simulated (a) phase tuning range and (b) gain tuning range when tuning the two 6-bit attenuator states in calibration block. The gain and phase differences are relative to the starting attenuator states at maximum attenuation.

IRR over frequency is expressed using (1) [11]

$$\mathrm{IRR}_{(f)} = -10\log\left(\frac{1+\alpha_{\epsilon(f)}{}^2 - 2\alpha_{\epsilon(f)}\cos\phi_{\epsilon(f)}}{1+\alpha_{\epsilon(f)}{}^2 + 2\alpha_{\epsilon(f)}\cos\phi_{\epsilon(f)}}\right) \quad (1)$$

where the errors in the USB and LSB frequencies are labeled $\alpha_{\epsilon(f)}$ and $\phi_{\epsilon(f)}$, for amplitude and phase, respectively. Thus, the goal of the calibration is to minimize these errors to maximize IRR. The calibration circuit samples part of the signal on the Q-path using Hybrid B. Hybrid A is included on the I-path, but serves no purpose except to minimize amplitude and phase imbalance. The calibration circuit acts as a modulator for the sampled error signals $\alpha_{\epsilon_u}|U|\angle 180° + \phi_{\epsilon_u}$ and $\alpha_{\epsilon_l}|L|\angle\phi_{\epsilon_l}$, although unlike a true vector modulator, the amplitude and phase transfer is not controlled independently and unilaterally. Two attenuators are used for amplitude weighting as in a typical vector-sum phase shifter and recombined using an RF balun to allow for phase inversion. Fig. 2(a) and (b) shows the simulated phase and amplitude shifts over the tuning range of the two 6-bit attenuators used for calibration. The modulated outputs are $\alpha_\kappa\alpha_{\epsilon_u}|U|\angle 180° + \phi_{\epsilon_u} + \phi_\kappa$ and $\alpha_\kappa\alpha_{\epsilon_l}|L|\angle\phi_{\epsilon_l} + \phi_\kappa$, where α_κ and ϕ_κ are the respective amplitude and phase changes resulting from the modulation (which is assumed identical for U and L to good approximation). These outputs are combined with the I-path via Splitter A to compensate for the phase and amplitude errors, resulting in the calibrated vectors $\alpha_{\Sigma_U}|U|\angle\phi_{\Sigma_U}$ and $\alpha_{\Sigma_L}|L|\angle\phi_{\Sigma_L}$. The calibration aims to minimize the phase and amplitude errors such that $\phi_{\Sigma_U}+\phi_{\epsilon_u}, \phi_{\Sigma_L}+\phi_{\epsilon_l} \to 0$ and $\alpha_{\Sigma_U}/\alpha_{\epsilon_u}, \alpha_{\Sigma_L}/\alpha_{\epsilon_l} \to 1$. The calibration is applied via the two 6-bit attenuator states a_1 and a_2.

B. Implementation

Prior to prototyping, the system was simulated in Cadence AWR Microwave office, including electromagnetic simulation of all distributed elements to consider all layout parasitics and nonideal S-parameter blocks for all SMD components, including those of the attenuators in different attenuation states. Equally important, a nonlinear simulation kit of the IQ mixer is used to model the spurious products in the downconverter more accurately by exploiting large signal circuit and system-level co-simulations. The system is implemented on Rodgers 4003C ($\epsilon_r = 3.55$) substrate with commercial off-the-shelf (COTS) products shown in Table I. The module is intended to operate at room temperature, postcryogenics, typically referred to as the warm cartridge assembly (WCA) in a radio astronomy receiver chain. This obviates the need for low noise and high gain, with the focus instead on frequency conversion. The downconverter is designed to cover an RF band of 18–45 GHz with an output IF of 4–11 GHz. The 18–45-GHz range is an application-driven band of interest over which image rejection is prioritized. Some gain variation over the band is, therefore, both expected and tolerable. Two fixed LO settings of 29 and 36 GHz are used to cover two 7-GHz bands from both the sidebands simultaneously. As an illustration, the LO setting at 29 GHz covers 18–25 GHz (LSB) and 32–40 GHz (USB), which allows for simultaneous observation of a methanol maser line at 23 GHz, and the four lines between 36 and 40 GHz. As discussed in Section II-A, calibration is performed via setting two digital attenuators that range from 0 to 31.5 dB.

TABLE I
COMPONENTS USED IN DOWNCONVERTER

Component	Product	Manufacturer	Package
3-dB Splitters	MPD-0226SM	Marki	SMT*
IQ Mixer	MMIQ-1865H	Marki	Bare Die
RF Hybrids	MQH-0517CH	Marki	Bare Die
RF Baluns	BAL-0416SMG	Marki	SMT
RF Attenuators	TGL2226-SM	Qorvo	SMT
Amplifiers	EHA-163L+	Mini-Circuits	SMT
BPF	Custom design [10]	-	-

*Surface Mount

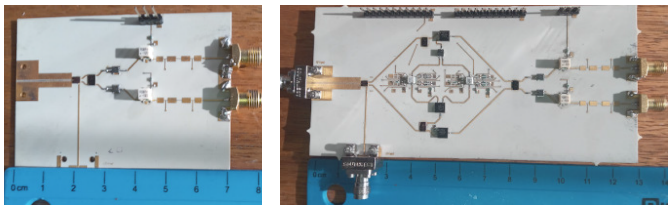

(a) (b)

Fig. 3. Photographs of 2SB downconverter prototypes. (a) Baseline (no calibration) and (b) with calibration.

III. MEASUREMENT RESULTS

The prototyped downconverter modules are shown in Fig. 3. Fig. 3(a) is the module without any calibration (baseline), and Fig. 3(b) is the module with calibration. All the measurements were carried out using an Anritsu ME7828A VNA, using the scalar mixer measurement application used to measure conversion gain of mixers and receivers. A multiplier (AT-AM4-2050-22T) and signal generator (MG37022A) were used to generate the LO signals at 29 and 36 GHz. For all the measurements, the RF power was set to −20 dBm with the LO power at +18 dBm (29 GHz) and +21 dBm (36 GHz). All the conversion measurements are performed with a 100-kHz IF bandwidth and 10-point averaging on the VNA. IRR is computed by measuring conversion gain at both the IF ports, and subsequently, the power ratio between the USB and LSB, with respect to the targeted RF sideband being injected. To calculate the image rejection of a given sideband,

Authorized licensed use limited to: University of Pretoria. Downloaded on January 15,2025 at 13:08:33 UTC from IEEE Xplore. Restrictions apply.

This article has been accepted for inclusion in a future issue of this journal. Content is final as presented, with the exception of pagination.

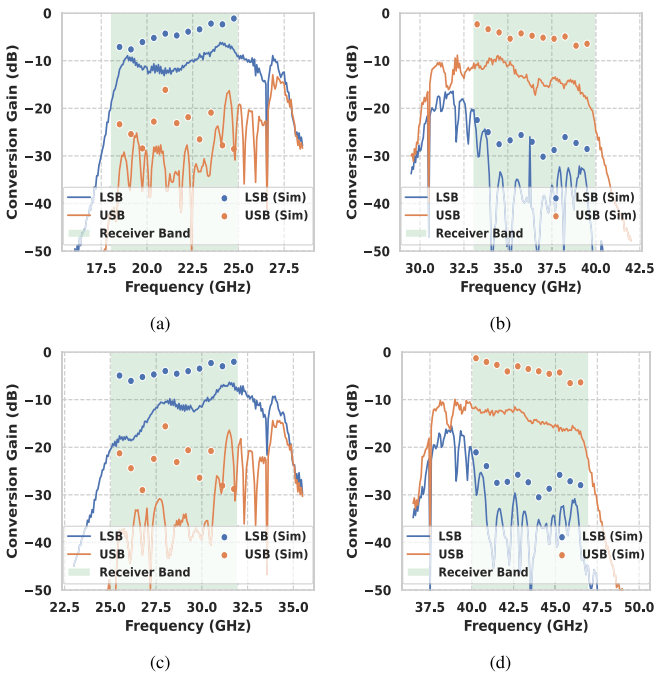

Fig. 4. Conversion gain measurements and simulations (Sim) for (a) LSB, LO = 29 GHz, (b) USB, LO = 29 GHz, (c) LSB, LO = 36 GHz, and (d) USB, LO = 36 GHz.

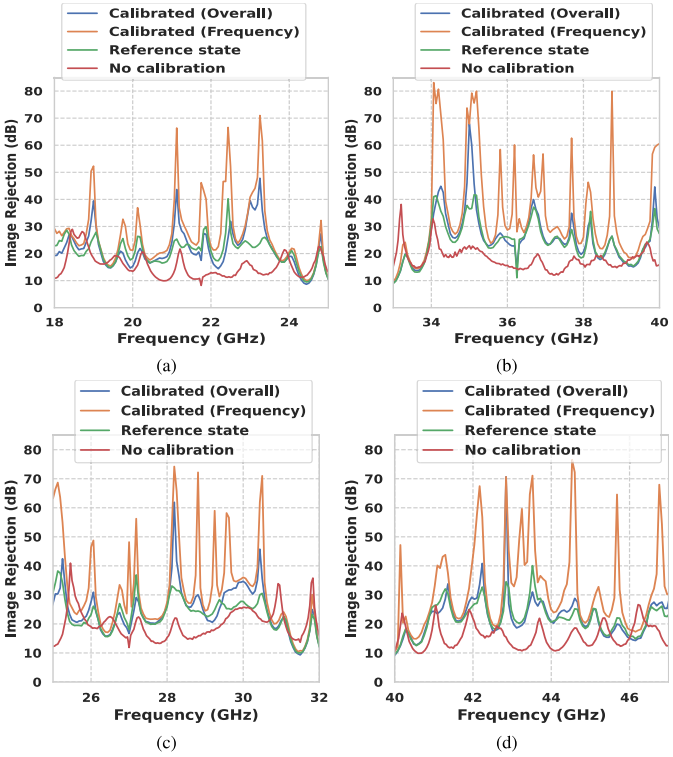

Fig. 5. Image rejection measurements for (a) LSB, LO = 29 GHz, (b) USB, LO = 29 GHz, (c) LSB, LO = 36 GHz, and (d) USB, LO = 36 GHz.

an USB and LSB signal is injected and calculated as

$$\mathrm{IRR_{USB}} = \mathrm{G_{USB}} - \mathrm{G_{LSB}} \tag{2}$$

$$\mathrm{IRR_{LSB}} = \mathrm{G_{LSB}} - \mathrm{G_{USB}} \tag{3}$$

where $\mathrm{G_{USB}}$ is the scalar USB gain in dB, and $\mathrm{G_{LSB}}$ the same for the LSB. For calibration measurements, a BeagleBone Black single board computer (SBC) was used to drive the two attenuators' digital inputs and store the conversion gain measurements for all attenuator state combinations.

Fig. 4 shows $\mathrm{G_{USB}}$ and G_{LSB} for 29- and 36-GHz LO settings, compared with the simulated results. The higher conversion loss, and standing wave pattern in the rejected band, would indicate that the 13 bondwire interconnects in the DUT have a greater impact on internal impedance mismatch and conversion loss than anticipated in simulation. Similarly, the equivalent measured IRRs are shown in Fig. 5 for the two LO settings. The graphs show the IRR of the calibrated circuit that minimizes IRR over the full band ("overall"), and compares it to the maximum attainable IRR at each frequency point ("frequency"), and zero calibration control ("reference state"). The IRR of the circuit without calibration circuit is also shown as "no calibration." In general, the globally optimized calibration shows an average of 9-dB improvement in IRR over the reference setting for both LO settings, with local optimization exceeding 40-dB IRR in places.

As shown in comparisons with previous works in Table II, the average IRR achieved in [2], [4], and [9] is higher (>30 dB) than the proposed solution, but over narrower bandwidths of up to 500 MHz compared with the 7-GHz achieved here. Prior works further require control of the digital backend, with [2] and [4] requiring postdigitization calibration and [9] requiring phase adjustment at quadrature generation. In contrast, the proposed technique offers stand-alone calibration for the IQ mixer, where a PCB implementation using off-the-shelf components can be used to improve image rejection without the need for a postdigitization algorithm at high IF frequencies or wide IF bandwidths.

TABLE II
COMPARISON TO SELECTED RECEIVERS/DOWNCONVERTERS WITH IRR IMPROVEMENT

Ref.	This Work	[2]	[4]	[9]
RF (GHz)	18–45	80–100	1.2–1.7	2.11–2.17
Fractional BW	86%	22%	34%	3%
IF (GHz)	4–11	DC–0.5	DC–0.5	DC
Technology	PCB (MCM)	Modules	PCB	0.25 μm CMOS
Post-Digitization Calibration	No	Yes	Yes	No*
IRR (dB)	>27#	>35	>50	>57
Type	2SB	2SB	2SB	Weaver

#Average values for each of the four bands.
*Improvement includes quadrature generation tuning before mixing.

IV. CONCLUSION

An 18–45-GHz 2SB downconverter image rejection calibration at RF is proposed. Measurements of the prototype MCM on RF PCB demonstrate its ability to improve image rejection over bandwidths of 7 GHz without the need to implement the quadrature hybrid digitally. The proposed downconverter is low-cost and suitable to mm-wave radio astronomy instruments performing simultaneous frequency observations. Future work will focus on microelectronic integration of the module.

ACKNOWLEDGMENT

The financial assistance of the South African Radio Astronomy Observatory (SARAO) toward this research is hereby acknowledged (www.sarao.ac.za).

Authorized licensed use limited to: University of Pretoria. Downloaded on January 15,2025 at 13:08:33 UTC from IEEE Xplore. Restrictions apply.

This article has been accepted for inclusion in a future issue of this journal. Content is final as presented, with the exception of pagination.

REFERENCES

[1] C.-C. Chiong et al., "Extended Q-band (eQ) receiver for Nobeyama 45-m telescope," *Proc. SPIE*, vol. 12190, Aug. 2022, Art. no. 121900M.

[2] R. Rodríguez, R. Finger, F. P. Mena, L. Bronfman, and E. A. Michael, "A digital sideband-separating receiver for the millimeter band," *Proc. SPIE*, vol. 9153, Jul. 2014, Art. no. 91532E.

[3] A. Kobak et al., "Multi-frequency VLBI observations of maser lines during the 6.7 GHz maser flare in the high-mass young stellar object G24.33+0.14," *Astron. Astrophys.*, vol. 671, p. 135, Mar. 2023.

[4] M. A. Morgan and J. R. Fisher, "Experiments with calibrated digital sideband-separating downconversion," *Publications Astronomical Soc. Pacific*, vol. 122, no. 889, pp. 326–335, Mar. 2010.

[5] E. M. Al Seragi, Y. L. Rajendra, W. Ahmad, M. Kaynak, P. F. Goldsmith, and S. Zeinolabdedinzadeh, "A 220–320 GHz high image rejection sideband separating receiver for space-borne observatories," *IEEE Trans. THz Sci. Technol.*, vol. 14, no. 2, pp. 162–177, Mar. 2024.

[6] F. Curotto et al., "Digital calibration test results for Atacama large millimeter/submillimeter array band 7+8 sideband separating receiver," *J. Astronomical Telescopes, Instrum., Syst.*, vol. 8, no. 2, pp. 1–10, Jun. 2022.

[7] E. T. R. Pinto, V. Tapio, and M. Juntti, "5G new radio compliant IQI compensation," *IEEE Wireless Commun. Lett.*, vol. 13, no. 2, pp. 407–411, Feb. 2024.

[8] T. Zhang, A. Najafi, M. Taghivand, and J. C. Rudell, "A precision wideband quadrature generation technique with feedback control for millimeter-wave communication systems," *IEEE Trans. Microw. Theory Techn.*, vol. 66, no. 1, pp. 215–226, Jan. 2018.

[9] L. Der and B. Razavi, "A 2-GHz CMOS image-reject receiver with LMS calibration," *IEEE J. Solid-State Circuits*, vol. 38, no. 2, pp. 167–175, Feb. 2003.

[10] S. Mundia and T. Stander, "Detailed design of an 18–45 GHz multi-purpose radio astronomy receiver," in *Proc. Int. Conf. Electromagn. Adv. Appl. (ICEAA)*, Sep. 2022, pp. 220–224.

[11] B. C. Henderson and J. A. Cook, "Image-reject and single-sideband mixers," Watkins-Johnson Company, Palo Alto, CA, USA, Tech. Note 3, 1985.

Authorized licensed use limited to: University of Pretoria. Downloaded on January 15,2025 at 13:08:33 UTC from IEEE Xplore. Restrictions apply.